IEEE Access
Multidisciplinary | Rapid Review | Open Access Journal

Received October 21, 2019, accepted November 25, 2019, date of publication December 3, 2019,
date of current version December 16, 2019.

Digital Object Identifier 10.1109/ACCESS.2019.2957272

Self-Mixing Interferometric Signal Enhancement Using Generative Adversarial Network for Laser Metric Sensing Applications

IMRAN AHMED, USMAN ZABIT, (Senior Member, IEEE), AND AHMAD SALMAN
School of Electrical Engineering and Computer Science, National University of Sciences and Technology (NUST), Islamabad 44000, Pakistan
Corresponding author: Ahmad Salman (ahmad.salman@seecs.edu.pk)

ABSTRACT Measurement performance of self-mixing interferometric (SMI) laser sensor can be significantly affected due to the presence of noise. In this case, conventional signal enhancement techniques yield compromised performance due to several limitations which include processing signals in frequency domains only, relying mainly on first order statistics, loss of important information present in higher frequency band and handling limited number of noise types. To address these issues, we propose a solution based on using generative adversarial network, a popular deep learning scheme, to enhance SMI signal corrupted with different noise types. Thus, taking advantage of the deep networks that can learn arbitrary noise distribution from large example set, our proposed method trains the deep network model end-to-end, able to process raw waveforms directly, learn 51 different noise conditions including white noise and amplitude modulation noise for 1,140 different types of SMI waveforms made up of 285 different optical feedback coupling factor (C) values and 4 different line-width enhancement factor α values. The results show that the proposed method is able to significantly improve the SNR of noisy SM signals on average of 19.49, 16.29, 10.34 dB for weak-, moderate-, and strong-optical feedback regime signals, respectively. For amplitude modulated SMI signals, the proposed method has corrected the amplitude modulation with maximum error (using area-under-the-curve based quantitative analysis) of 0.73% for SMI signals belonging to all optical feedback regimes. Thus, our proposed method can effectively reduce the noise without distorting the original signal. We believe that such a unified and precise method leads to enhancement of performance of SMI laser sensors operating under real-world, noisy conditions.

INDEX TERMS Interferometry laser sensors, self-mixing signal enhancement, vibration measuring laser sensors, waveform enhancement, generative adversarial network (GAN), signal noise removal, neural network for signal enhancement.

I. INTRODUCTION

Self-mixing or optical feedback interferometry based laser diode sensors [1]–[3] are being increasingly used for metric sensing applications due to their low-cost, auto-aligned and compact nature [4], [5]. Multiple SMI applications such as micro-displacement measurement [6], measurement of rotation angles (yaw and pitch) [7], detection of single micro-particles in airflow [8], displacement measurement in resonant gyroscopes [9], acquisition of arterial pulse wave [10], Young's modulus measurement [11], measurement of rotational speed of servo drives [12], measurement of size of Brownian particles [13] and carriers density imaging [14] have been demonstrated. However, the performance of SMI sensors can significantly degrade due to presence of various noise sources encountered during real-world, experimental conditions. For example, accurate measurement of vibration using conventional laser diode based sensor becomes a challenge [15].

The experimentally acquired SMI signal can be affected by white noise, as shown in Figure 1. Various factors contribute white noise to SMI signals such as fluctuations in temperature, current, and voltage of the laser diode, photodiode, and related biasing and amplifying electronic circuits. In addition to white noise, another factor that distorts the shape of SMI signal is known as amplitude modulation noise

The associate editor coordinating the review of this manuscript and approving it for publication was Vicente Alarcon-Aquino.

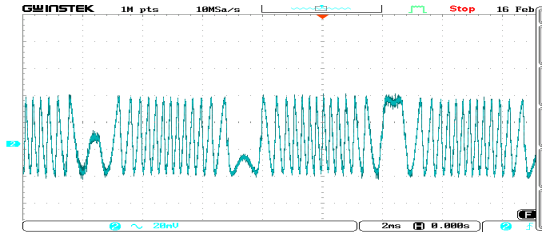

FIGURE 1. Experimental self-mixing signal distorted with simple white noise.

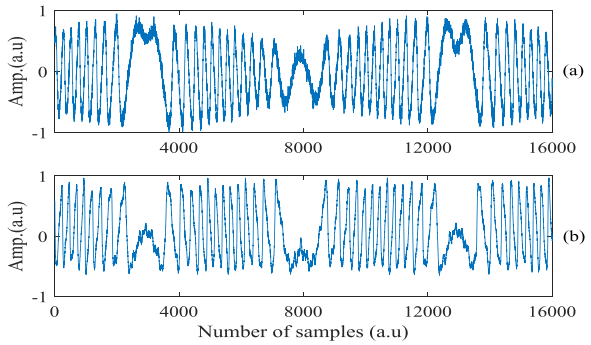

FIGURE 2. Experimental self-mixing signal (SMI). (a) SMI signal distorted with amplitude modulation noise i.e., amplitude of SMI signal is enclosed in an envelope. (b) SMI signal distorted with amplitude noise i.e., variation in amplitude of SMI signal at every instant.

(see Figure 2) [15], caused due to the rough target surface [16]. Furthermore, SMI signals have been reported to be affected by transient oscillations [17] and laser mode-hopping as well [20], [21]. Thus, under such conditions, accurate SMI sensing and measurement are compromised. For example, SMI displacement measurement performance is severely affected, primarily because of difficulty in detecting the white noise affected SMI fringes whose amplitude also begins to vary [24]. Various specialized fringe detection methods have thus been reported to mitigate this situation [25]–[27].

The shape of SMI signals usually varies by changing the values of coupling factor C and line-width enhancement factor α [18], therefore, SMI signals have been reported to divide into three main optical feedback regimes i.e., weak-($0.1 < C < 1$), moderate-($1 < C < 4.6$) and strong-optical feedback regime ($C > 4.6$) [19]. In order to improve the performance of SMI laser vibration sensor, various pre-processing techniques have been presented which should be applied before undertaking the fringe detection [20]–[23]. However, in general, these methods are limited to remove only white noise for specific cases such as weak feedback regime [22], to some extent, moderate feedback regime [20], [21] but unable to accurately work for strong feedback regime [20]–[23]. More importantly, to the best of authors' knowledge, correction of SMI signal's amplitude distortion has not been previously proposed.

Conventional techniques, such as those utilizing band-pass filtering to remove white noise, may lead to the loss of important information present in higher frequency band

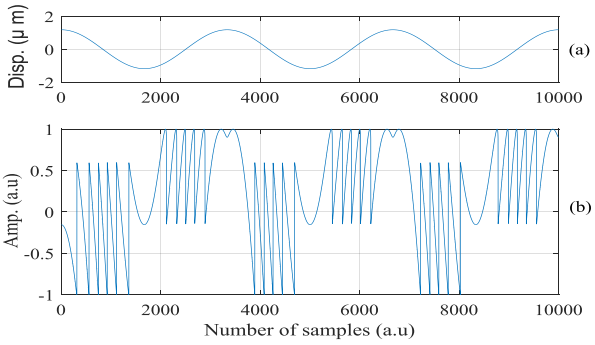

FIGURE 3. SMI signal with parameters line-width enhancement factor $\alpha = 4$, feedback level factor $C = 4$ for a moving target. (a) Target vibration in micrometers. (b) Periodic variation of optical output power (known as SMI signal).

of SMI signal leading to signal distortion (specifically in case of moderate- and strong-optical feedback regime) [22]. Moreover, under real-world operating conditions, the optical feedback regime of SMI signal can change at any instant, and in each case, the corresponding SMI signal will have different spectral properties [22]. Therefore, in order to remove white noise from experimental signals, the conventional techniques required a continuous adjustment of the noise suppression filters for each optical feedback regime.

In this paper, a machine learning based solution for SMI signal enhancement is proposed by recognizing the statistical nature of white noise and more complex amplitude modulation noise. We have employed generative adversarial network (GAN) [28] as a generic yet single module to take distorted SMI signal as input and generate noise- and distortion-free output without any prior assumption on the type of noise and optical feedback regime. This enables us to apply a trained GAN system to denoise the SMI signal such that the target displacement retrieval with high accuracy can be subsequently achieved.

II. THEORY OF SMI

A. SMI SIGNAL

The SMI occurs when a portion of emitted laser light reflects back from a remote target (undergoing displacement $D(t)$) and couples into the active laser cavity. The re-injected laser light then interferes with the field inside the laser cavity [29]. This ''self-mixing'' causes a variation of different laser parameters including wavelength as well as optical output power (OOP) as a function of $D(t)$ due to the changes in the optical path length D_0 and the so-called external laser cavity. In this work, time-varying OOP signal $P(t)$ (acquired using the built-in photo-diode) is used and is denoted as the SMI signal, as shown in Figure 3.

Typical setup of a SMI sensing system consists of a laser source, lens and an external remote target, as shown in Figure 4. This SMI signal ($P(t)$) is then fed to signal acquisition unit and is finally processed by a computer for the sake of target motion information extraction through SMI signal ($P(t)$) [3].

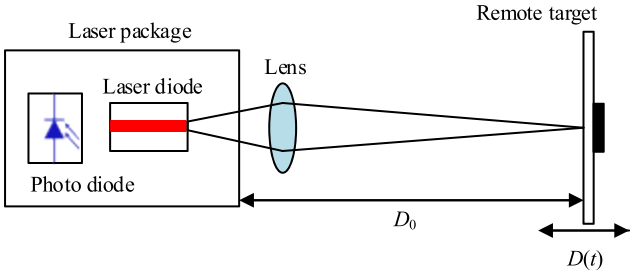

FIGURE 4. Basic setup of self-mixing interferometry laser vibration sensing system.

B. DISPLACEMENT RETRIEVAL FROM SMI SIGNAL

The most common and simplest way of retrieving the target displacement from SMI laser sensor is to use a well-known theoretical model developed by Lang and Kobayashi in [30] where the variations of optical output power $P(t)$, acquired from the laser diode (see Figure 3 (b)) under feedback phase $\phi_f(t)$, can be written as given in [29].

$$P(t) = P_0(1 + m.\cos(\phi_f(t))). \tag{1}$$

where, feedback phase or rough phase $\phi_f(t)$ can be extracted by rearranging (1) and the relation between target displacement $D(t)$ and feedback phase $\phi_f(t)$ is given by

$$\phi_f(t) = \frac{2\pi D(t)}{\lambda_f/2}. \tag{2}$$

Equation (2) cannot be used directly to retrieve the target displacement. In order to do so, smooth phase $\phi_f(t)$ is required to be estimated. Thus, the laser wavelength under feedback $\lambda_f(t)$ can be found by solving the corresponding laser phase equation (1)

$$\phi_0(t) = \phi_f(t) + C.\sin(\phi_f(t) + \arctan(\alpha)). \tag{3}$$

However, the optimal estimation of the two key parameters i.e., C and α are also required in calculating the smooth phase $\phi_0(t)$ [29]. Finally, $D(t)$ can be retrieved by using

$$\phi_0(t) = \frac{2\pi D(t)}{\lambda_0/2}. \tag{4}$$

The parameters in the above equations are summarized in Table 1.

The relationship of C is given by [29] as

$$C = \frac{\tau_D}{\tau_L}\gamma\sqrt{1 + \alpha^2\kappa_{ext}}. \tag{5}$$

C plays an important role in SMI because it directly affects the shape of the signal and is usually used to classify the operating optical feedback regime between weak, moderate and strong optical feedback [19].

In order to retrieve the displacement of remote target by using SMI laser vibration sensor, it is necessary to further process the SMI signal by using one of the many existing signal processing method, for example, phase unwrapping method (PUM) [4], which helps in retrieving the displacement information of remote target from acquired SMI signal.

TABLE 1. Physical meaning of parameters.

Parameters Used In Equations (1)-(4)	
α	Line-width Enhancement Factor
C	Optical feedback Level Factor
$\phi_0(t)$	Phase without optical feedback
$\phi_f(t)$	Phase with optical feedback
$D(t)$	Distance between laser and target
λ_0	Wavelength of LD under free running condition
λ_f	Wavelength subjected to optical feedback
P_0	Optical power in free running state
m	Modulation index
τ_L	Round trip time in internal cavity
τ_D	Round trip time in external cavity
γ	Coupling efficiency
κ_{ext}	Surface reflection coefficient of target body

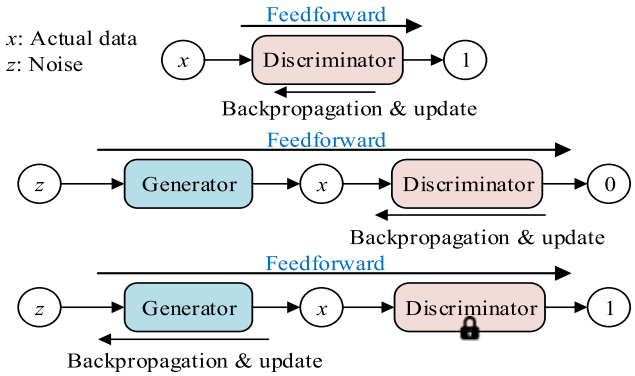

FIGURE 5. Adversarial training of GAN.

However, noisy signal may result in poor phase extraction and consequently affect the retrieved target displacement. Therefore, noisy SMI signal must be cleaned before applying phase unwrapping method to get smooth phase.

To summarize, we need to perform the following signal processing before applying PUM on SMI signal for the accurate retrieval of displacement from SMI laser sensor. The first step of signal processing consists of rough estimation of of $\phi_f(t)$ from $P(t)$ as per (1). Then, the task is to recover $\phi_0(t)$ by using $\phi_f(t)$ as mentioned in (3). This is followed by estimation of C and α parameters. However, to recover $\phi_0(t)$ by using $\phi_f(t)$ is a tedious process when $P(t)$ is noisy as this may lead to incorrect rough estimation of $\phi_f(t)$ which in turn results in inaccurate recovery of $\phi_0(t)$ [15]. Hence, an appropriate pre-processing of $P(t)$ is required in order to get accurate target displacement. Therefore, we choose a neural network based technique i.e., GAN [28] to achieve this task which is discussed in detail in the following section.

III. PROPOSED METHOD

GAN, a deep convolutional neural network, works with a simple encoder-decoder technique in unsupervised learning paradigm [31]. GAN has been used in several image generation, classification and speech enhancement tasks with promising results on complex data [32]–[34]. Therefore, with a similar motivation, we have applied GAN to improve the

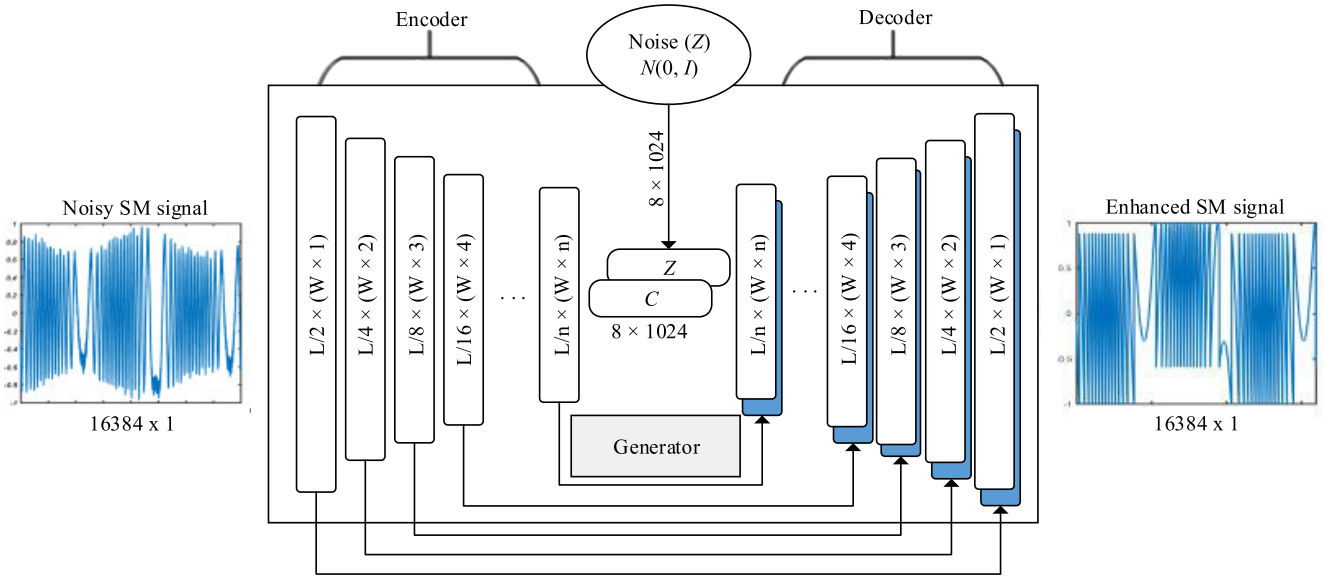

FIGURE 6. Architecture of GAN used for SMI signal enhancement.

quality of SMI waveforms corrupted with noise. The proposed system has advantages of quick processing of waveforms, works end-to-end on raw data and does not require explicit feature extraction from data [28], [34]. Moreover, it learns from various type of SMI signal under different noise conditions.

A. GAN ARCHITECTURE

The GAN architecture consists of two components, a generator and a discriminator, denoted by G and D respectively [28]. The network learns to map random noise vector z and observed SMI signal x to an enhanced output SMI signal y i.e., $G : \{x, z\} \rightarrow y$. Off the two key components, the generator performs mapping and learns to generate the enhanced SMI signal y while keeping in view those enhanced SMI signals that must be similar to the observed signals x. The second key component is discriminator that acts as a classifier to classify the output y of generator either as real or fake signal [28]. Both GAN components work together in an adversarial training fashion where discriminator always tries to classify the output y coming from the generator as fake. In contrast, generator updates its parameters and tries to produce output y such that the discriminator should classify it as a real signal. As a result of this training in a continuous feedforward and backpropagation passes, discriminator D learns to discriminate between the fake and the real signal. On the other hand, generator G tunes its parameters to generate output waveform that is closer to the real data [34]. Basic working of adversarial training of GAN is explained in Figure 5.

In order to achieve this adversarial training, a specific criterion is chosen in [28], which can be written as

$$minmaxA(D, G) = E[\log D(y) + E[\log(1 - D(G(z)))]. \quad (6)$$

Later on, a new conditioned version of GAN is introduced to stabilize the system [32], [33]. In conditional GAN, the input x is added to the above equation and hence becomes

$$minmaxA(D, G) = E[\log D(x, y)] + E[\log(1 - D(x, G(x, z)))]. \quad (7)$$

To improve the generated sample of G and training stabilization of GAN, least squares GAN (LSGAN) is developed in [35] where (7) becomes

$$minA_{LSGAN}(D) = \frac{1}{2}E[(D(x, y) - 1)^2] + \frac{1}{2}E[(D(x, G(x, z)))^2]. \quad (8)$$

$$minA_{LSGAN}(G) = \frac{1}{2}E[(D(x, G(x, z)) - 1)^2]. \quad (9)$$

To get more accurate and realistic results of adversarial component, L1 norm is shown to be very effective [35] and is controlled by a parameter λ. This results in a change in (9) i.e.,

$$minA_{LSGAN}(G) = \frac{1}{2}E[(D(x, G(x, z)) - 1)^2] + \lambda \mid\mid G(x, z) - z \mid\mid \quad (10)$$

In order to implement the above described GAN for SMI signal enhancement problem, we downsample the noisy SMI signal to 16 kHz, yielding approximately 16,384 samples per second as followed in [34]. Then, together with the latent vector z, it is applied to G, which is used to produce enhanced SMI signal. The architectures of both G and D for this work are adopted from those in [34].

The working principle of G in the GAN resembles an autoencoder as shown in Figure 6. In encoding stage, the noisy input SMI signal of size $16,384 \times 1$ is compressed to $8 \times 1,024$ when it passes through 22 one-dimensional convolutional layers with filter width of 31 and stride of 2

followed by parametric rectified linear units (PReLUs) [34]. Here, the latent vector z of size $8 \times 1,024$ sampled from a normal distribution $N(0,I)$ is concatenated with the thought vector C. This concatenated vector is then passed to the decoding stage. The decoder architecture D is basically in reverse to that of generator with the same number of filter layers and filter width. However, it uses two input channels made up of $16,384$ samples and virtual batch-norm [37] before LeakyReLU nonlinearities with $\alpha = 0.3$. The last activation layer is composed of one-dimensional convolution layer with a single filter of width 1. Therefore, it results in a reduced number of parameters from $8 \times 1,024 = 8,129$ to $8 \times 1 = 8$ for fully-connected final classification layer [34]. In order to achieve stabilization, strided layers are used in G rather than other pooling approaches [31] and additionally, skip connections are utilized within D, where each layer in encoding stage is connected to its corresponding layer in decoding stage. Skip connections helps in avoiding the compression at the middle stage of the model and pass the fine-grain information of SMI signal such as phase and alignment to the decoder, resulting in improved performance.

In training GAN, values of some other hyperparameter are required to be selected based on cross-validation for optimum performance. We selected λ for loss function to be 90, learning rate for both D and G networks is chosen to be 0.002, total number of epochs is set to 63 with batch size of 50. In training phase, our algorithm uses the sliding window to extract the chunks of SMI signal of $1s$ duration for every $0.5s$ shift i.e., each window contains 16,384 samples with 50% overlap with adjacent window. However, during testing the window without overlap is used for whole length of SMI signal, a scheme followed in [34].

Training GAN architecture requires large dataset containing SMI signals. We divided our dataset into two subsets: 1) training set and 2) test set. The training set is further split into two more components i.e., noisy training set containing noise-free data and clean training set, which comprises the same signal but corrupted with noise. For training the GAN, both noisy and clean training sets are fed to the network as shown in Figure 7. Similarly, the test set is also divided into two categories known as noisy test set and clean test set, which also acts as ground truth. In order to test the performance, the noisy test set is applied to the GAN as input. Subsequently, the ground truth waveforms in clean test set are then compared with the output of GAN (filtered data) and gets the error signal which helps in judging the performance of the proposed system.

Our proposed system is developed in Tensorflow version 1.1.0$rc1$. Some other packages include Python 3.5, Numpy 1.12.1, Scipy 0.18.1, Toml 0.9.2, CUDA 8.0 and CuDNN $v5.1$ are also used.

IV. DATASET

In order to validate the proposed method we have perform various simulations under different noise conditions. In this work, two types of cases based on two noise conditions are addressed, first is white noise and the other is amplitude modulation noise.

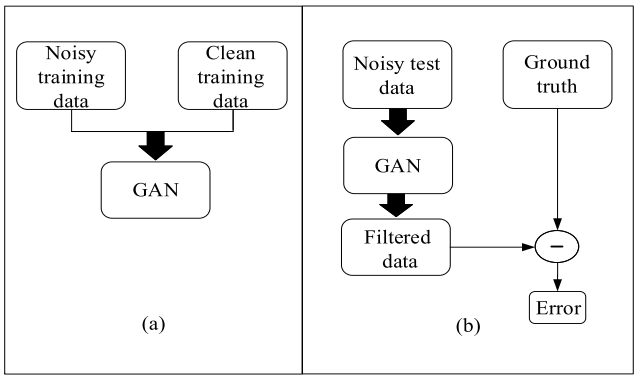

FIGURE 7. Data preparation for GAN (a) Training phase (b) Testing phase.

For additive white noise removal, the large simulated dataset is prepared for training and testing the GAN model. The training dataset consist of 5,400 while testing dataset contain 80 examples of SMI signals. To introduce variation in the dataset, we choose different combinations of C, α and SNR. The parameter C ranges from [0 to 10], α ranges from [3 to 7] and SNR was taken with values [30, 27, 25, 23, 20, 17, 15, 13, 10] dBs. Therefore, these three parameters contributes with 150, 4 and 9 different values to constitute $150 \times 4 \times 9 = 5,400$ SMI signal examples. For preparing test dataset, we considered 10 different values of C, 2 values for α and 4 different SNR values in the range of [29, 21, 14, 9] dBs to make a total of $10 \times 2 \times 4 = 80$ SMI signals.

In order to remove the amplitude modulation noise from SMI signal, we separately train and test the GAN model on dataset which consists of SMI signals distorted with amplitude modulation noise. Thus, a simulated dataset of SMI signals (with 5,670 training and 392 test examples) distorted with amplitude modulation noise is prepared. Various type of amplitude modulation tones are generated in simulation and then integrated with the original SMI signals in order to mimic the practical scenario. For training dataset, we choose 135 different values of C which range from [0 to 10], $\alpha = 4.5$ and 6 different SNR values of [25, 23, 20, 17,15,13] dBs with 7 various type of amplitude modulation tones. This sums up to $135 \times 1 \times 6 \times 7 = 5,670$ SMI signals. On the other hand, test dataset is made up of 14 different values of C, $\alpha = 4.5$, 4 different SNR values of 11, 16, 19, and 24 dBs and 7 various type of amplitude modulation tones to create a total of $14 \times 1 \times 4 \times 7 = 392$ SMI signals

V. RESULTS

A. REMOVAL OF WHITE NOISE

The GAN is first trained on simulated training dataset of 5,400 SMI signals and then the model is tested on the simulated test dataset of 80 SMI signals. In this case, the results in terms of SNR quantification are presented in Table 2 and Table 3. The scores shows that the proposed system proves

TABLE 2. Quantitative analysis of GAN performance in terms of SNR for SMI signals with fixed $\alpha = 4.5$ distorted with additive white noise.

Fixed α value $= 4.5$									
η = SNR of Noisy SMI signals									
ψ = SNR of Filtered SMI signals									
Improved SNR $= \Delta = \psi - \eta$									
C	$\eta = 29$ dB	$\eta = 21$ dB	$\eta = 14$ dB	$\eta = 9$ dB	$\eta = 29$ dB	$\eta = 21$ dB	$\eta = 14$ dB	$\eta = 9$ dB	Average of Δ
	Values of ψ in dBs				Values of Δ in dBs				
0.02	43.14	40.57	35.77	32.08	14.14	19.57	21.77	23.80	19.41 dB
0.33	42.72	42.86	36.75	31.29	13.27	21.86	22.57	22.29	
0.83	39.87	41.4	34.28	31.19	10.87	20.40	20.28	22.19	
1.62	36.85	34.14	31.57	26.34	07.85	13.14	17.57	17.34	15.78 dB
2.24	40.44	34.76	33.24	31.37	11.44	13.76	19.24	22.37	
3.11	41.35	40.72	31.52	26.15	12.35	19.72	17.52	17.15	
4.98	36.17	33.56	30.85	24.8	07.17	12.56	16.85	15.80	09.36 dB
6.85	33.12	32.95	29.33	25.01	04.12	11.95	15.33	16.01	
8.95	36.79	30.23	21.81	22.23	07.79	09.23	07.81	13.23	
9.75	28.38	23.66	19.32	13.56	-0.62	02.66	05.32	04.56	

TABLE 3. Quantitative analysis of GAN performance in terms of SNR for SMI signals with fixed $\alpha = 6.5$ distorted with additive white noise.

Fixed α value $= 6.5$									
η = SNR of Noisy SMI signals									
ψ = SNR of Filtered SMI signals									
Improved SNR $= \Delta = \psi - \eta$									
C	$\eta = 29$ dB	$\eta = 21$ dB	$\eta = 14$ dB	$\eta = 9$ dB	$\eta = 29$ dB	$\eta = 21$ dB	$\eta = 14$ dB	$\eta = 9$ dB	Average of Δ
	Values of ψ in dBs				Values of Δ in dBs				
0.02	44.11	41.51	35.52	32.20	15.11	20.51	21.52	23.20	19.57 dB
0.33	44.80	41.07	37.62	32.07	15.80	20.07	23.62	23.07	
0.83	40.50	39.08	34.07	31.36	11.50	18.08	20.07	22.36	
1.62	36.82	36.06	32.17	26.12	07.82	15.06	18.17	17.12	16.78 dB
2.24	40.83	40.14	34.50	28.61	11.83	19.14	20.50	19.61	
3.11	42.70	39.69	34.04	28.88	13.70	18.69	20.04	19.88	
4.98	37.40	35.61	30.95	24.13	08.40	14.61	16.95	15.13	11.32 dB
6.85	34.28	33.73	29.47	26.62	05.28	12.73	15.47	17.62	
8.95	37.11	31.01	31.85	21.14	08.11	10.01	17.85	12.14	
9.75	29.19	23.57	28.02	19.10	0.19	02.57	14.02	10.10	

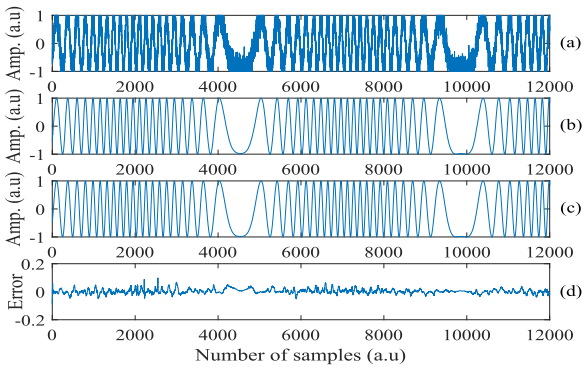

FIGURE 8. Results of denoising of SMI signal distorted with simple white noisy for weak feedback regime with $C = 0.02$, $\alpha = 6.5$ and SNR = 9 dB. (a) Noisy SMI Signal. (b) Filtered SMI signal after passing through GAN. (c) Ground truth. (d) Error signal i.e., difference between filtered and ground truth SMI signal.

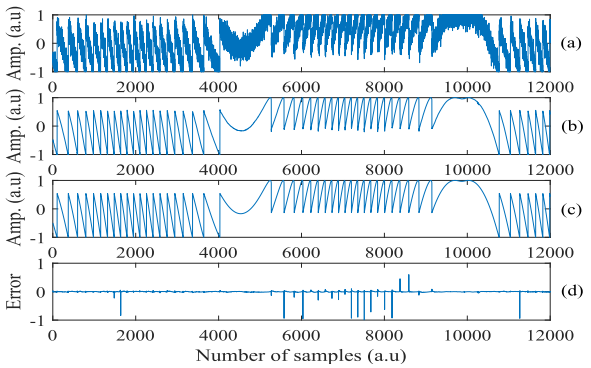

FIGURE 9. Results of denoising of SMI signal distorted with simple white noisy for moderate feedback regime with $C = 3$, $\alpha = 4.5$ and SNR = 9 dB. (a) Noisy SMI Signal. (b) Filtered SMI signal after passing through GAN. (c) Ground truth. (d) Error signal.

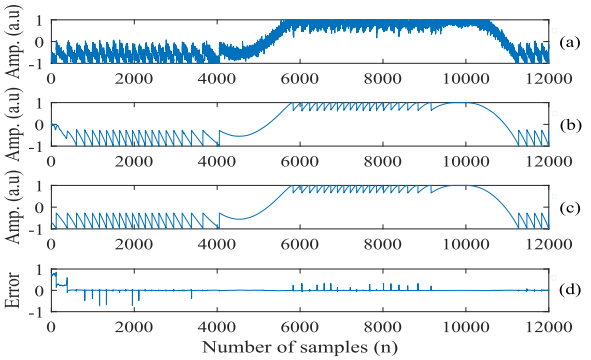

FIGURE 10. Results of denoising of SMI signal distorted with simple white noisy for strong feedback regime $C = 9.75$, $\alpha = 4.5$ and SNR = 14 dB. (a) Noisy SMI Signal. (b) Filtered SMI signal after passing through GAN. (c) Ground truth. (d) Error signal.

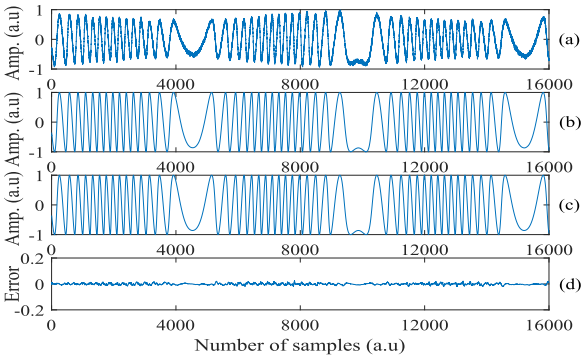

FIGURE 11. Results of denoising of SMI signal distorted with amplitude modulation and white noise for weak feedback regime with $C = 0.33$, $\alpha = 4.5$ and SNR = 24 dB. (a) Noisy SMI Signal. (b) Filtered SMI signal after passing through GAN. (c) Ground truth. (d) Error signal.

to be beneficial for improving the SNR in SMI signals as it is successful in reducing noise for all feedback regimes. However, with increasing the value of C from weak to stronger feedback regime, the performance is comparatively degraded. The proposed network performed well not only for weak feedback regime but also for moderate and strong feedback regimes, which is a complex case in the previous works [21], [22]. Figure 8, 9 and 10 depicts the performance in terms of signal representation for weak, moderate and strong feedback regimes respectively. It is evident that additive white noise in SMI signals is significantly reduced and sharp transitions in each fringe remain unchanged when compared with the ground truth. The results are shown for various C, α and SNR values. More importantly, in comparison to the previous work, our proposed method is performing superior in many ways, for example, for weak and moderate feedback regime, the error plots in Figure 8(d) and Figure 9(d) have far less amplitude as compare to the one reported in [21]. Also, the SMI signal in our case is contaminated with more noise, having SNR = 9 dB as compare to 20 dB in [21].

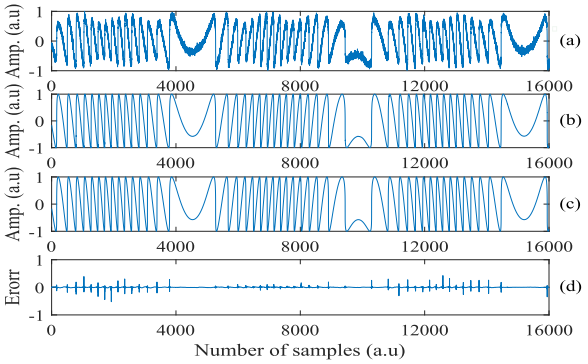

FIGURE 12. Results of denoising of SMI signal distorted with amplitude modulation and white noise for moderate feedback regime $C = 1.01$, $\alpha = 4.5$ and SNR = 19 dB. (a) Noisy SMI Signal. (b) Filtered SMI signal after passing through GAN. (c) Ground truth. (d) Error signal.

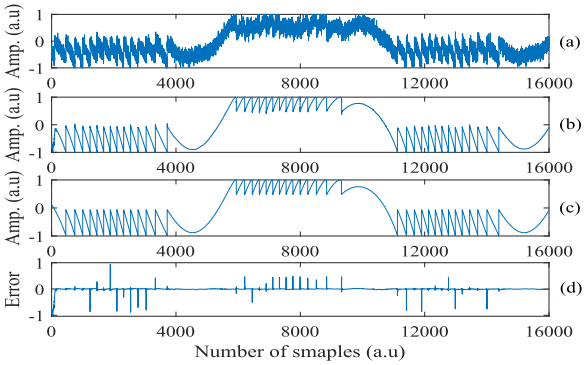

FIGURE 13. Results of denoising of SMI signal distorted with amplitude modulation and white noise for strong feedback regime $C = 6.8$ $\alpha = 4.5$ and SNR = 11 dB. (a) Noisy SMI Signal. (b) Filtered SMI signal after passing through GAN. (c) Ground truth. (d) Error signal.

Moreover, [21], [22] are unable to denoise the SMI signals that lies in strong feedback regime. In contrast, our proposed method can handle this challenge even in the presence of higher noise with SNR = 14 dB as shown in Figure 10.

B. REMOVAL OF AMPLITUDE MODULATION NOISE

As mentioned earlier, SMI signals are contaminated with many types of noises in which one of the most complex case is the corruption with amplitude modulation noises. This results in a poor retrieval of target displacement. Therefore, it is imperative to achieve reasonable SMI signal enhancement in this case.

The evaluation scale for modulation denoising using the proposed system is chosen to be area under the curve (AUC) instead of SNR because our aim is to check the extent of demodulation achieved by the GAN. AUC of the modulated signal is always less than the AUC of the filtered and the ground truth SMI signal as shown in Figure 14. In order to find AUC, modulated SMI signal is first divided in two part from zero baseline i.e., into positive and negative cycles. The trapezoidal rule is then applied to calculate the overall AUC by adding the value of positive cycle with the absolute value of negative cycle. Same steps are followed to find the AUC

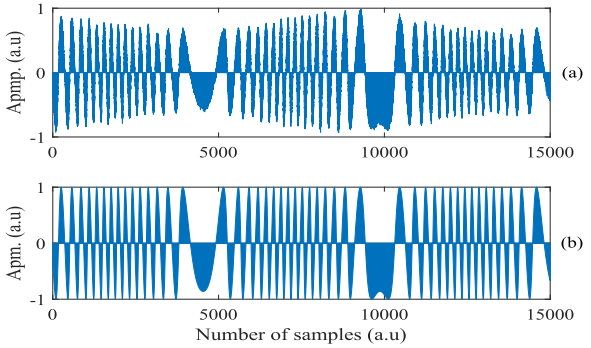

FIGURE 14. Area under the curve (AUC) for SMI signal with parameter $C = 0.33$, $\alpha = 4.5$ SNR = 24 dB (a) AUC = 6,603 for amplitude modulated SMI signal (b) AUC = 9,578 for filtered SMI signal.

TABLE 4. Quantitative analysis of GAN performance in terms of area under the curve (AUC) for SMI signals distorted with amplitude modulation noise.

Fixed α value = 4.5							
AUCG	Area under curve for groundtruth SMI signal						
AUCM	Area under curve for modulated SMI signal						
AUCF	Area under curve for filtered SMI signal						
DR	% Demodulation required = (AUCG − AUCM)/AUCG × 100						
DA	% Demodulation achieved = (AUCF − AUCM)/AUCG × 100						
E	% Error = (AUCG − AUCF)/AUCG × 100 = DR − DA						
Sr. No	C	AUCM	AUCG	AUCF	DR	DA	E
1	0.02	6991	9736	9685	28.19%	27.67%	0.52%
2	0.15	6964	9700	9647	28.21%	27.66%	0.55%
3	0.33	6938	9638	9568	28.01%	27.29%	0.73%
4	0.63	6857	9527	9465	28.03%	27.37%	0.65%
5	0.97	6788	9413	9344	27.89%	27.15%	0.73%
6	1.01	6744	9401	9340	28.26%	27.61%	0.65%
7	1.28	6628	9011	8988	26.45%	26.19%	0.26%
8	2.43	5041	7076	7035	28.76%	28.18%	0.58%
9	3.4	5395	7155	7104	24.60%	23.89%	0.71%
10	4.82	5655	7556	7555	25.16%	25.15%	0.01%
11	5.3	5649	7803	7771	27.60%	27.19%	0.41%
12	6.8	6347	8812	8755	28.16%	27.50%	0.65%
13	7.2	6501	8867	8825	26.81%	26.33%	0.48%
14	8.7	5845	9165	9102	36.48%	35.78%	0.69%

for filtered and ground truth SMI signal. We have evaluate this scale on different test SMI signals and lists the numerical result in Table 4. The % error (E) between demodulation achieved (DA) and demodulation required (DR) in last column of Table 4 shows the high accuracy of our proposed technique as it has corrected the amplitude modulation with maximum error of 0.73% for SMI signals belonging to all feedback regimes.

Figure 11, 12 and 13 show some examples of SMI signal denoising with weak, moderate and strong feedback regimes respectively. For case of weak feedback regime, Figure 11(a) shows the amplitude of noisy SMI signal distorted by a modulation envelope. This modulated signal is then rectified after passing through the GAN and amplitude of spikes can be seen in Figure 11(b), which approach the maxima $[-1, 1]$ without distorting the original shape of the signal. As a result, the corresponding error signal with insignificant amplitude is observed. In the case of more challenging moderate and strong feedback regimes, the amplitude distortion can be seen at every instant as shown in Figure 12(a) and Figure 13(a). However, favourable results with minimum error can still be obtained using GAN denoising as depicted in Figure 12(b, d) and Figure 13(b, d). To the best of our knowledge such cases were not analyzed in previous studies. Therefore, our

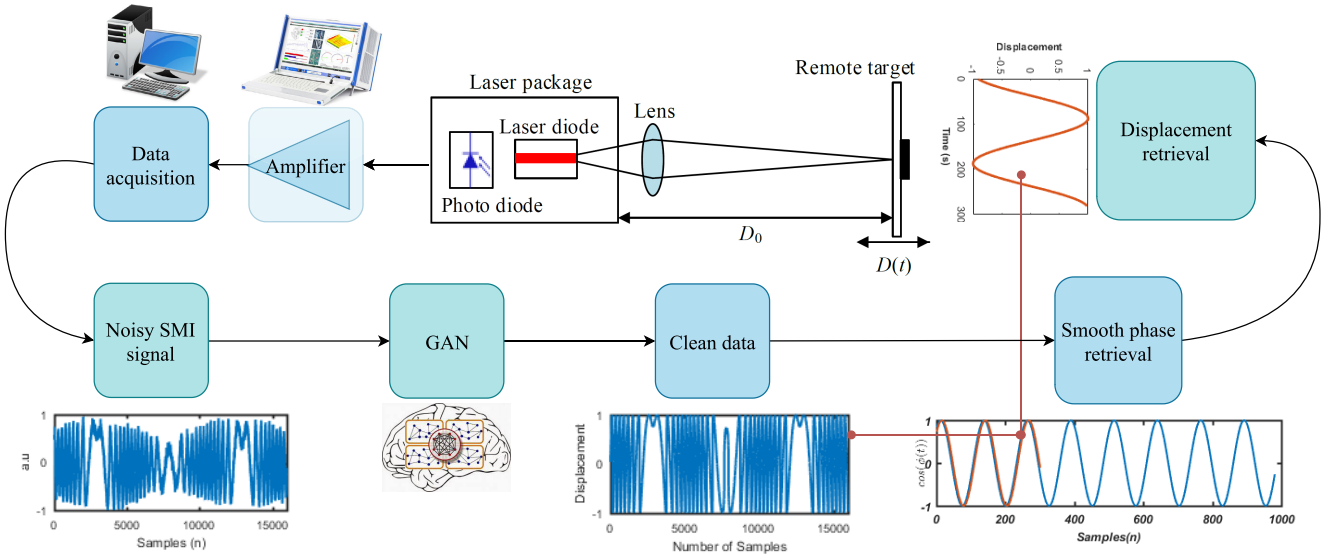

FIGURE 15. Schematic diagram for the experimental setup of the proposed method.

proposed method successfully solves the moderate and strong feedback regime signals distorted with additive white noise as well as signals distorted with amplitude modulation noise.

C. DENOISING EXPERIMENTAL SIGNAL

To validate the effectiveness of our proposed method, we also report the results on actual SMI signals acquired in the laboratory. In the experimental setup, a loud speaker is used as moving target that is driven by simple sine wave with a constant frequency. The laser diode model DL-7140 is used, which is biased with a DC current of 90 mA and operated at room temperature (25°C).

The experimental configuration is outlined and explained in Figure 15. In the first step, the noisy SMI signal corrupted with white and amplitude modulation distortion is acquired via photo diode (PD), the noisy signal is then amplified by using transimpedance amplifier and passed through the data acquisition unit. The amplified noisy SMI signal is then applied to the GAN. At this stage, the pre-trained GAN yields a noise-free SMI signal which is further processed using the phase unwrapping technique to get a smooth phase signal. The denoising/rectification result of experimental SMI signal is shown in Figure 16. The top plot in Figure 16 shows the SMI signal corrupted with amplitude modulation as well as additive white noise and its denoised version is shown in the bottom plot. The result shows that white noise and modulation effects are significantly diminished while keeping the shape of the transition of fringes unchanged. On quantitative analysis in terms of AUC, we have found that the proposed method has improved the AUC = 6,591 (for noisy SMI signal in top plot of Figure 16) to AUC = 9,119 (for denoised SMI signal in bottom plot of Figure 16), which indicates the high accuracy of the proposed method.

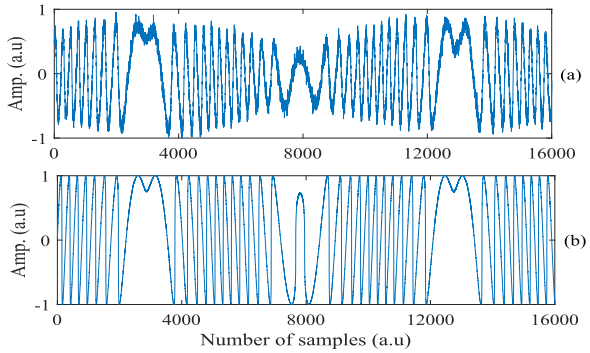

FIGURE 16. Experimentally acquired SMI signal in laboratory (a) Signal distorted with amplitude modulation as well as white additive noise. (b) Denoised signal using GAN.

VI. CONCLUSION

In this work, we have proposed a new pre-processing technique to enhance the quality of SMI signal corrupted with white and amplitude modulation noise in all major optical feedback regimes (weak, moderate and strong). The proposed method works end-to-end directly on raw SMI data and implemented within a generative adversarial framework. Since the model works as an encoder-decoder hierarchy with fully convolutional structure, it can quickly process the SMI signal segments to remove noise without introducing any artifacts in the rectified signals. Results indicate that the proposed method has provided on average improvement in SNR of 19.49, 16.29, 10.34 dB for weak, moderate and strong optical feedback regime SMI signals respectively. For amplitude modulated SMI signals, the proposed method has corrected the amplitude modulation with maximum error (using area-under-the-curve based quantitative analysis) of 0.73% for all optical feedback regimes. GAN-based denoising of SMI

signals is effective and successful as the system learns the statistical pattern of various noises and avoids the use of conventional signal processing approaches which compromise on their performance for every new distortion example. Hence, using GAN, we can improve the performance of SMI sensor, which directly depends on the quality of the SMI signal.

REFERENCES

[1] M. Norgia, F. Bandi, A. Pesatori, and S. Donati, "High-sensitivity vibrometer based on FM self-mixing interferometry," in *Proc.J. Phys., Conf. Ser.*, 2019, vol. 129, no. 1, Art. no. 012020.

[2] S. Donati, "Developing self-mixing interferometry for instrumentation and measurements," *Laser Photon. Rev.*, vol. 6, no. 3, pp. 393–417, 2012.

[3] T. Taimre, M. Nikolić, K. Bertling, Y. L. Lim, T. Bosch, and A. D. Rakić, "Laser feedback interferometry: A tutorial on the self-mixing effect for coherent sensing," *Adv. Opt. Photon.*, vol. 7, no. 3, pp. 570–631, 2015.

[4] A. Ehtesham, U. Zabit, O. D. Bernal, G. Raja, and T. Bosch, "Analysis and implementation of a direct phase unwrapping method for displacement measurement using self-mixing interferometry," *IEEE Sensors J.*, vol. 17, no. 22, pp. 7425–7432, Nov. 2017.

[5] Z. A. Khan, U. Zabit, O. D. Bernal, M. O. Ullah, and T. Bosch, "Adaptive cancellation of parasitic vibrations affecting a self-mixing interferometric laser sensor," *IEEE Trans. Instrum. Meas.*, vol. 66, no. 2, pp. 332–339, Feb. 2017.

[6] H. Wang, Y. Yu, J. Xi, Q. Guo, and J. Tong, "A self-mixing laser diode for micro-displacement measurement," in *Proc. IEEE Int. Freq. Control Symp. (IFCS)*, Olympic Valley, CA, USA, May 2018, pp. 1–4.

[7] S. Ottonelli, F. D. Lucia, M. D. Vietro, M. Dabbicco, G. Scamarcio, and F. P. Mezzapesa, "A compact three degrees-of-freedom motion sensor based on the laser-self-mixing effect," *IEEE Photon. Technol. Lett.*, vol. 20, no. 16, pp. 1360–1362, Aug. 15, 2008.

[8] V. Contreras, J. Lönnqvist, and J. Toivonen, "Detection of single microparticles in airflows by edge-filter enhanced self-mixing interferometry," *Opt. Express*, vol. 24, no. 8, pp. 8886–8894, 2016.

[9] G. He, R. Gordenker, J.-K. Woo, J. A. Nees, B. Shiari, T. Nagourney, J.-Y. Cho, and K. Najafi, "Laser self-mixing interferometry for precision displacement measurement in resonant gyroscopes," in *Proc. IEEE Int. Symp. Inertial Sensors Syst. (INERTIAL)*, Naples, FL, USA, Apr. 2019, pp. 1–4.

[10] A. Arasanz, F. J. Azcona, S. Royo, A. Jha, and J. Pladellorens, "A new method for the acquisition of arterial pulse wave using self-mixing interferometry," *Opt. Laser Technol.*, vol. 63, pp. 98–104, Nov. 2014.

[11] K. Lin, Y. Yu, J. Xi, Q. Guo, J. Tong, and H. Li, "Young's modulus measurement using fibre-coupled self-mixing laser diode," in *Proc. Int. Conf. Numer. Simulation Optoelectron. Devices (NUSOD)*, Sydney, NSW, Australia, Jul. 2016, pp. 157–158.

[12] H. Sun, J. Liu, Q. Zhang, and R. Kennel, "Self-mixing interferometry for rotational speed measurement of servo drives," *Appl. Opt.*, vol. 55, no. 2, pp. 236–241, 2016.

[13] S. Sudo, Y. Miyasaka, K. Otsuka, Y. Takahashi, T. Oishi, and J. Ko, "Quick and easy measurement of particle size of Brownian particles and plankton in water using a self-mixing laser," *Opt. Express*, vol. 14, no. 3, pp. 1044–1054, 2006.

[14] L. L. Columbo, F. P. Mezzapesa, M. Dabbicco, M. Brambilla, G. Scamarcio, and M. S. Vitiello, "Carriers density imaging by self-mixing interferometry in a THz quantum cascade laser," in *Proc. IEEE SENSORS*, Nov. 2014, pp. 754–757.

[15] C. Zhao, M. Norgia, and K. Li, "Balanced detection for self-mixing interferometry to improve signal-to-noise ratio," *Proc. SPIE*, vol. 10619, Jan. 2018, Art. no. 1061902.

[16] S. Donati and G. Martini, "3D Profilometry With a Self-Mixing Interferometer: Analysis of the Speckle Error," *IEEE Photon. Technol. Lett.*, vol. 31, no. 7, pp. 545–548, Apr. 1, 2019.

[17] Z. Liu, Y. Yu, Y. Fan, J. Xi, Q. Guo, and J. Tong, "Eliminating influence of transient oscillations on a self-mixing interferometry," *Opt. Eng.*, vol. 55, no. 10, 2016, Art. no. 104102.

[18] C. Kim, C. Lee, and O. Kwonhyok, "Effect of linewidth enhancement factor on fringe in a self-mixing signal and improved estimation of feedback factor in laser diode," *IEEE Access*, vol. 7, pp. 28886–28893, 2019.

[19] O. D. Bernal, U. Zabit, and T. M. Bosch, "Robust method of stabilization of optical feedback regime by using adaptive optics for a self-mixing micro-interferometer laser displacement sensor," *IEEE J. Sel. Topics Quantum Electron.*, vol. 21, no. 4, pp. 336–343, Jul. 2015.

[20] Y. Sun, Y. Yu, and J. Xi, "Wavelet transform based de-noising method for self mixing interferometry signals," *Proc. SPIE*, vol. 8351, Jan. 2012, Art. no. 83510G.

[21] L. Wei, J. Chicharo, Y. Yu, and J. Xi, "Pre-processing of signals observed from laser diode self-mixing intereferometries using neural networks," in *Proc. IEEE Int. Symp. Intell. Signal Process.*, Oct. 2007, pp. 1–5.

[22] X. Zhang, J. Xi, Y. Yu, and J. Chichero, "The Fourier spectrum analysis of optical feedback self-mixing signal under weak and moderate feedback," in *Proc. 4th IEEE Int. Symp. Electron. Design, Test Appl.*, Hong Kong, Jan. 2008, pp. 481–495.

[23] Y. Yu, T. Mei, J. Xi, J. F. Chicharo, H. Ye, and Z. Wang, "Eliminating noises contained in sensing signals from a self-mixing laser diode," *Proc. SPIE*, vol. 7656, 2010, Art. no. 76560E.

[24] O. D. Bernal, H. C. Seat, U. Zabit, F. Surre, and T. Bosch, "Robust detection of non-regular interferometric fringes from a self-mixing displacement sensor using Bi-wavelet transform," *IEEE Sensors J.*, vol. 16, no. 22, pp. 7903–7910, Nov. 2016.

[25] M. U. Zabit, O. D. Bernal, G. Raja, and T. Bosch, "Detection of multimodal fringes for self-mixing-based vibration measurement," *IEEE Trans. Instrum. Meas.*, to be published.

[26] A. Magnani, A. Pesatori, and M. Norgia, "Self-mixing vibrometer with real-time digital signal elaboration," *Appl. Opt.*, vol. 51, no. 21, pp. 5318–5325, Jul. 2012.

[27] A. L. Arriaga, F. Bony, and T. Bosch, "Speckle-insensitive fringe detection method based on Hilbert transform for self-mixing interferometry," *Appl. Opt.*, vol. 53, no. 30, pp. 6954–6962, 2014.

[28] I. Goodfellow, J. Pouget-Abadie, M. Mirza, B. Xu, D. Warde-Farley, S. Ozair, A. Courville, and Y. Bengio, "Generative adversarial nets," in *Proc. Adv. Neural Inf. Process. Syst.*, 2014, pp. 2672–2680.

[29] I. Ahmed and U. Zabit, "Fast estimation of feedback parameters for a self-mixing interferometric displacement sensor," in *Proc. Int. Conf. Commun., Comput. Digit. Syst. (C-CODE)*, Islamabad, Pakistan, Mar. 2017, pp. 407–411.

[30] R. Lang and K. Kobayashi, "External optical feedback effects on semiconductor injection laser properties," *IEEE J. Quantum Electron.*, vol. 16, no. 3, pp. 347–355, Mar. 1980.

[31] A. Radford, L. Metz, and S. Chintala, "Unsupervised representation learning with deep convolutional generative adversarial networks," in *Proc. Int. Conf. Learn. Represent. (ICLR)*, 2015, pp. 1–15.

[32] P. Isola, J.-Y. Zhu, T. Zhou, and A. A. Efros, "Image-to-image translation with conditional adversarial networks," 2016, *arXiv:1611.07004*. [Online]. Available: https://arxiv.org/abs/1611.07004

[33] J. Gauthier, "Conditional generative adversarial nets for convolutional face generation," in *Proc. Class Project Stanford CS231N: Convolutional Neural Netw. Vis. Recognit.*, 2014, pp. 1–9.

[34] S. Pascual, A. Bonafonte, and J. Serrà, "SEGAN: Speech enhancement generative adversarial network," 2017, *arXiv:1703.09452*. [Online]. Available: https://arxiv.org/abs/1703.09452

[35] X. Mao, Q. Li, H. Xie, R. Y. K. Lau, Z. Wang, and S. P. Smolley, "Least squares generative adversarial networks," 2016, *arXiv:1611.04076*. [Online]. Available: https://arxiv.org/abs/1611.04076

[36] K. He, X. Zhang, S. Ren, and J. Sun, "Delving deep into rectifiers: Surpassing human-level performance on imagenet classification," in *Proc. IEEE Int. Conf. Comput. Vis. (ICCV)*, Dec. 2015, pp. 1026–1034.

[37] T. Salimans, I. Goodfellow, W. Zaremba, V. Cheung, A. Radford, X. Chen, and X. Chen, "Improved techniques for training GANs," in *Proc. Adv. Neural Inf. Process. Syst.*, 2016, pp. 2226–2234.

IMRAN AHMED received the bachelor's degree in electrical engineering from Riphah International University, Islamabad, Pakistan. He is currently pursuing the master's degree with the School of Electrical Engineering and Computer Science, National University of Sciences and Technology, Islamabad. His research interests include signal processing, machine learning, and optoelectronics.

USMAN ZABIT (M'12–SM'19) received the Ph.D. degree from the Institut National Polytechnique Toulouse (INPT), France, in 2010. He is currently an Associate Professor with the National University of Sciences and Technology (NUST), Islamabad, Pakistan. He was a recipient of the Prix Leopold Escande 2010 and the European Mechatronics Award from INPT and European Mechatronics Meeting, in 2010.

AHMAD SALMAN received the master's degree in electrical engineering from the National University of Sciences and Technology (NUST), Islamabad, Pakistan, and the Ph.D. degree from The University of Manchester, U.K., with specialization in machine learning and signal processing. He is currently an Assistant Professor with the School of Electrical Engineering and Computer Science, NUST. He is leading the Optimization and Machine Learning Research Group.